Biosensors and Bioelectronics 185 (2021) 113267

Contents lists available at ScienceDirect

Biosensors and Bioelectronics

journal homepage: www.elsevier.com/locate/bios

Erythrocyte-camouflaged biosensor for α-hemolysin detection

Insu Kim [a,1], Yonghwan Kim [a,b,1], Sang Won Lee [a], Dongtak Lee [a], Hyo Gi Jung [a,b], Jae Won Jang [a,b], Taeha Lee [c,d], Young Kyung Yoon [e,***], Gyudo Lee [c,d,**], Dae Sung Yoon [a,b,*]

[a] School of Biomedical Engineering, Korea University, Seoul 02841, South Korea
[b] Interdisciplinary Program in Precision Public Health, Korea University, Seoul 02841, South Korea
[c] Department of Biotechnology and Bioinformatics, Korea University, Sejong 30019, South Korea
[d] Interdisciplinary Graduate Program for Artificial Intelligence Smart Convergence Technology, Korea University, Sejong 30019, South Korea
[e] Division of Infectious Diseases, Department of Internal Medicine, Korea University College of Medicine, Seoul 02841, South Korea

ARTICLE INFO

Keywords:
Biosensor
Cell membrane
Erythrocyte
α-hemolysin
Electrochemical impedance spectroscopy

ABSTRACT

Without appropriate treatment, *Staphylococcus aureus* (*S. aureus*) infection can cause life-threatening diseases (e.g., meningitis, pneumonia, bacteremia, and sepsis). However, a rapid and accurate point-of-care test for the infection remains challenging. The bacterium secretes α-hemolysin (Hla), which spontaneously binds to the cell membrane of erythrocyte, and eventually lyses the cell *via* pore formation. Taking advantage of this phenomenon, we apply the erythrocyte membrane (EM) extracted from human whole blood as a novel bioreceptor for detecting Hla, fabricating erythrocyte-camouflaged biosensors (ECB) by coating EM onto electrochemical impedance electrodes. We verify the existence of EM on the ECB by using confocal microscopy and atomic force microscopy. We demonstrate that ECBs sensitively detect Hla spiked in phosphate buffer saline and human serum. Also, the sensor shows higher sensitivity to Hla than major blood proteins, such as human serum albumin, fibrinogen, and gamma globulin. Specifically, the signal intensities for Hla are 8.8–12.7 times higher than those in the same concentration of those blood proteins. The detection limit of the ECB for Hla is 1.9 ng/ml while the dynamic range is 0.0001–1 mg/ml. Finally, we validate the constant sensing performance of ECB with 99.0 ± 5.6% accuracy for 35 days of storage.

1. Introduction

S. aureus is a commensal and pathogenic bacterium that can cause a wide range of clinical infections. It is a leading cause of bacteremia, mild infections, and life-threatening conditions, such as sepsis and endocarditis (Tong et al., 2015). While the pathogenic bacterium can be neutralized through antibiotics, bacteria became antibiotic resistant by gene transfer and natural selection (Foster 2017; Turner et al., 2019). In particular, methicillin-resistant *S. aureus* (MRSA) prevails because of multiple drug resistance to beta-lactam antibiotics. Also, it is reported that MRSA is one of the most common pathogens isolated from surgical site infection (Sun et al., 2019). Therefore, in monitoring hospital-acquired infection, rapid and accurate detection of *S. aureus* is an important issue for the treatment of patients with infectious diseases and in-hospital infection control.

To diagnose the bacteria infection, several techniques have been devised. Real-time polymerase chain reaction (RT-PCR) is based on the quantification of fluorescence produced by a reporter molecule, which is amplified by each PCR cycle. While it is considered that the RT-PCR is reliable and rapid, it is necessary to have several pretreatment processes, such as bacteria separation in blood by differential centrifugation, and DNA extraction (Cattoir et al., 2011). Enzyme-linked immunosorbent assay (ELISA) was introduced to detect the bacteria. Although ELISA is highly reliable, it requires time, analytical devices, and experts (Sekiguchi et al., 1995). In turn, it is impossible to utilize either method for bacteria detection as point-of-care testing.

α-hemolysin (Hla), an exotoxin of *S. aureus*, is well-known as a pore-forming toxin which is able to cause the lysis of erythrocytes (red blood cells) (Evans et al., 2013; Soule et al., 1959). In detail, secreted Hla monomers diffuse to the susceptible cells and bind to them to form

* Corresponding author. School of Biomedical Engineering, Korea University, Seoul 02841, South Korea.
** Corresponding author. Department of Biotechnology and Bioinformatics, Korea University, Sejong 30019, South Korea.
*** Corresponding author.
E-mail addresses: young7912@korea.ac.kr (Y.K. Yoon), lkd0807@korea.ac.kr (G. Lee), dsyoon@korea.ac.kr (D.S. Yoon).
[1] These authors contributed equally to this work.

https://doi.org/10.1016/j.bios.2021.113267
Received 18 September 2020; Received in revised form 14 April 2021; Accepted 16 April 2021
Available online 23 April 2021

ring-shaped pores by oligomerization themselves. The pore facilitates the permeation of essential molecules, ions, and water, resulting in osmotic phenomena, cell depolarization, and cell death (Yadav et al., 2008). It has been well researched that the Hla spontaneously binds erythrocyte and forms pore-forming heptamers, resulting in hemolysis. Also, it is reported that erythrocyte expresses Hla receptor which is allowed to bind EM specifically (Divyakolu et al., 2019). Various cell membranes are formed into vesicles, which coated on nanoparticles or solid surfaces, due to disassembly and reassembly *via* hemolysis and sonication. Using these mechanisms, Zhang and his group reported that EM-coated nanoparticles can neutralize toxic Hla in blood (Esteban-Fernández de Ávila et al., 2018; Hu et al., 2013). Also, it was reported that lipid membrane could be functionalized on solid surfaces including glass and silicon oxide wafers, through vesicle fusion and solvent-assisted methods (Ferhan et al., 2019; Mingeot-Leclercq et al., 2008). Moreover, as a bioreceptor, EM is more cost-effective than Hla-specific antibodies, because it can be easily extracted and obtained from human whole blood (Kim et al., 2018). In this regard, we speculated that EM-coated biosensor enables the direct detection of Hla to monitor the bacterial infection.

In this study, we developed erythrocyte-camouflaged biosensor (ECB), where the surface of the working electrode was functionalized with a single layer of EM (Kim et al., 2021). The EM coating was verified by electrochemical impedance spectroscopy (EIS), fluorescent microscopy, contact angle analysis, scanning electron microscopy (SEM), and atomic force microscopy (AFM). The electrochemical properties of ECB were characterized by cyclic voltammetry (CV). The sensing performance, such as the detection range, limit-of-detection (LOD) in 3σ, and stability, was examined. It is demonstrated that the sensor was extremely sensitive (LOD = 1.9 ng/ml), and selective against major blood proteins, such as human serum albumin (HSA), fibrinogen (Fib), and gamma globulin (GG). Then, ECB was verified with Hla-spiked human serum. Finally, ECB was highly stable for 35 days, and was able to measure Hla with 99.0 ± 5.6% accuracy.

2. Materials and methods

2.1. Materials and reagents

Human serum albumin (HSA), fibrinogen from human plasma (Fib), γ-globulin (GG) from human blood, α hemolysin (Hla), sulfuric acid, 18:0 1,2-distearoyl-sn-glycero-3-phosphoethanolamine-N-[methoxy (polyethylene glycol)-2000] (PEG2000-PE), 18:1 1,2-dioleoyl-sn-glycero-3-phosphoethanolamine-N-(carboxyfluorescein) (PE-CF), potassium chloride, ferricyanide $[Fe(CN)_6]^{3-}$, and ferrocyanide $[Fe(CN)_6]^{4-}$ were purchased from Sigma-Aldrich. Phosphate buffer saline (PBS, pH 7.4) and distilled water were purchased from Gibco. Screen-printed gold electrode (Counter: Pt; Ref.: Ag) was purchased from DropSens (DRP-250AT, Spain). Single-donor human whole blood was purchased from Innovative Research (USA).

2.2. Extraction of the erythrocyte membrane

EM was extracted from human whole blood stored in K2EDTA vacuum tube (BD Vacutainer, lavender). The following steps were conducted at 4 °C. Erythrocyte were isolated from whole blood, and washed 3 times with ice-cold 1 × PBS by centrifugation at 200×*g* for 5 min. Erythrocytes were hemolyzed *via* suspending hypotonic solution (ice-cold 0.25 × PBS) for 30 min. The hemolyzed suspension containing EM fragments was collected and purified by centrifugation at 20,000×*g* for 30 min, to eliminate free hemoglobins. The light pink sediment of EM concentrate was collected, and stored at −80 °C, until use.

2.3. Preparation of the ECB

Screen-printed gold electrodes were activated *via* cyclic voltammetry with 0.5 M sulfuric acid. The potential was cycled 12 times from −0.4 to 1.4 V (vs. Ag/AgCl) with scan rate of 100 mV/s, to achieve a stable peak current. The chloroform solubilizing PEG2000-DPPC was evaporated under nitrogen stream and dried in a desiccator under vacuum for 10 min. PEG2000-DPPC was resuspended in distilled water at 0.1 mM final concentration and added to 1000-fold diluted EM concentrate (0.1%), and vigorously mixed. Then, the PEG2000-DPPC and EM mixture was sonicated for 3 min to form EM vesicles (Escajadillo et al., 2017; Gao et al., 2013). The vesicles were placed on gold electrode, and heated at 50 °C for 30 min, to form supported lipid bilayer *via* membrane fusion (Kim et al., 2020; Mingeot-Leclercq et al., 2008). To remove residual EM vesicles, the ECBs were washed with distilled water, and dried in a clean bench.

2.4. Verification and characterization of the ECBs

EM coating was verified by electrochemical impedance spectroscopy (EIS) and confocal microscopy. EIS was conducted to validate the EM coating incubated for 0–30 min. The EM vesicles were placed onto working electrode of the screen-printed sensor, and incubated for 30 min. To remove residual EM vesicles, the sensors were washed with distilled water, and the charge transfer resistant (R_{ct}) increment analyzed. For the fluorescent image, PE-CF (0.1 mM) was added to the EM vesicles, sonicated for 3 min to intercalate the PE-CF to EM vesicles, and coated onto the working electrode as described in section 2.3. For the stability test of ECB, we coated the surface of working electrode with the solution which was prepared by mixing 0.1% of EM and 10 μM of green fluorescent (i.e., carboxyfluorescein). The electrodes were stored at 4 °C, and the stability was observed for 35 days. For visualization of the ECBs, scanning electron microscopy (SEM) and atomic force microscopy (AFM) were conducted. The hydrophilicity of ECBs was evaluated *via* contact angle of 10 μl of distilled water. The electrochemical properties of ECBs were characterized by cyclic voltammetry (CV) and EIS.

2.5. Hla measurement

Hla, dissolved in PBS with various concentrations of 0.0001–1 mg/ml, was placed on the working electrode of ECBs, and incubated for 30 min at 37 °C. Unbound Hla was removed from ECBs by gentle washing. To measure R_{ct}, EIS was conducted with 1 × PBS containing 0.1 M KCl and 0.5 mM $[Fe(CN)_6]^{3-/4-}$ in the frequency range of 0.5–100 kHz, and a signal amplitude of 10 mV. R_{ct} was attained from Nyquist plot. The selectivity of ECB was demonstrated measuring 0.01 mg/ml of Fib, HSA, and GG, *via* the same procedure used for measuring Hla. The R_{ct} increments of each protein were normalized for comparison.

2.6. Clinical sample test

Blood samples from 5 patients with *S. aureus* bacteremia and from 4 patients without *S. aureus* bacteremia were collected in a blood culture bottles (BACTEC; Becton Dickinson, Sparks, MD, USA) and stored at −4 °C before use. The isolation and identification were performed using the Microscan WalkAway 96 plus system (Siemens Healthcare Diagnostics, Berkeley, CA), and confirmed by matrix-assisted laser desorption ionization–time of flight mass spectrometry (Bruker Daltonics, Bremen, Germany). The institutional Review Board (IRB) of the Korea University Anam Hospital approved the protocol and waived the need for informed consent (institutional review board registration no. 2020AN0526). To test clinical samples, each of 9 blood samples was centrifuged at 3000×*g* for 10 min and diluted 100 times with 1 × PBS. It was placed on the working electrode of ECBs, and incubated for 30 min at 37 °C. After incubation, ECBs were gently washed and measured.

2.7. Instrumentation

Confocal laser scanning microscopy (FV1000, Olympus, Japan) was employed to verify EM functionalization on ECB. The surface of ECBs was visualized by scanning electron microscopy (JSM-6701 F, Jeol, Japan) and atomic force microscopy (NX10, Park Systems, Korea). The AFM images were attained using non-contact mode with non-contact cantilever with force constant of 42 N/m and resonant frequency of 330 kHz (NCHR, Nanosensors, Switzerland). The roughness of AFM images was calculated using SmartScan software. The contact angle was measured using contact angle analyzer (Pheonix150, Surface Electro Optics, Korea), and calculated *via* Surfaceware software. The electrochemical characterization was conducted using potentiostat (VersaSTAT3, Princeton Applied Research, USA). Both experiments were performed in PBS (pH 7.4) containing 0.1 M KCl and 0.5 mM $[Fe(CN)_6]^{3-/4-}$ at 25 °C. CV was conducted in the potential range of −0.1 to 0.5 V and scan rate of 10–250 mV/s.

3. Results and discussion

3.1. Fabrication of the ECB and a principle of Hla detection

Screen-printed gold electrode was activated by potential cycling in 0.5 M sulfuric acid, until a stable CV was achieved (Fig. S1) (Fischer et al., 2009; González-Sánchez et al., 2019). The working electrode was coated with EM containing 5% PEG 2000. Here, the PEG is able to act as a spacer, which allows mimicking of the intracellular space (cytoplasm) (Tanaka and Sackmann 2005). Thus, the space allows Hla to penetrate EM, without spatial interference of the electrode surface (Castellana and Cremer 2006). Also, the PEGylation of pure lipids enables vesicle fusion on gold surface (Tabaei et al., 2014). The EM was coated by the vesicle fusion method, which was modified from our previous work (Kim et al. 2018, 2019; Mingeot-Leclercq et al., 2008). Briefly, the collected EM concentrate was diluted in distilled water, mixed with PEG2000-PE, and sonicated to form PEGylated EM vesicles (Kumar et al., 2019). The EM vesicles were placed on the working electrode of bare biosensors, and incubated at 50 °C for 30 min, to transform the EM vesicles to planar PEG-supported EM layer (Scheme 1a and b). It is considered that the *S. aureus* toxin, Hla, spontaneously binds onto ECBs by identifying the surface of ECBs as erythrocyte (Scheme 1c) (Hu et al., 2013). Then, the charge transfer resistance (R_{ct}) of ECBs increases, corresponding to the number of Hla bound onto the sensors (Scheme 1d–f). The inset of Scheme 1d illustrates the Randles circuit, which is an equivalent circuit with mixed kinetic and charge-transfer control (Russell et al., 2019). The circuit for analyzing impedance spectra consists of four main structures: electrolyte resistance (R_s), charge transfer resistance (R_{ct}), Warburg impedance (Z_w), and double-layer capacitance (C_{dl}). Using the EIS, we could detect Hla through the changes of impedance (i.e., R_{ct}). Here, R_{ct} was sequentially increased by coating the EM on working electrode, and Hla on ECB.

3.2. Optimization and verification of the EM coating

To optimize the incubation time for EM coating, the EM vesicles were placed onto working electrodes, and incubated for 0–30 min at 50 °C. The R_{ct} increments (ΔR_{ct}) were observed with time *via* EIS (Fig. 1a). We verified that the R_{ct} was increased to 12.6 ± 0.8 Ohm, and saturated after 20 min. The result represents that the working electrodes of ECB were fully coated with a 30 min-incubation (Park et al., 2019). Also, the EM coating was validated by fluorescence imagery (Fig. 1b–d). PE-CF, fluorescence-labeled lipid, was inserted into EM vesicles, before coating. Then, the vesicles were placed on the working electrode of sensors, and incubated for 0 and 30 min. After 30 min of incubation, the green fluorescence at 525 nm was observed to cover the whole surface. The surface of working electrodes covered by EM was examined with SEM, which demonstrated that the surface became even (Fig. S2). As a result, we confirmed that the ECBs incubated for 30 min were fully covered by EM. To verify the surface hydrophilicity, the contact angle of

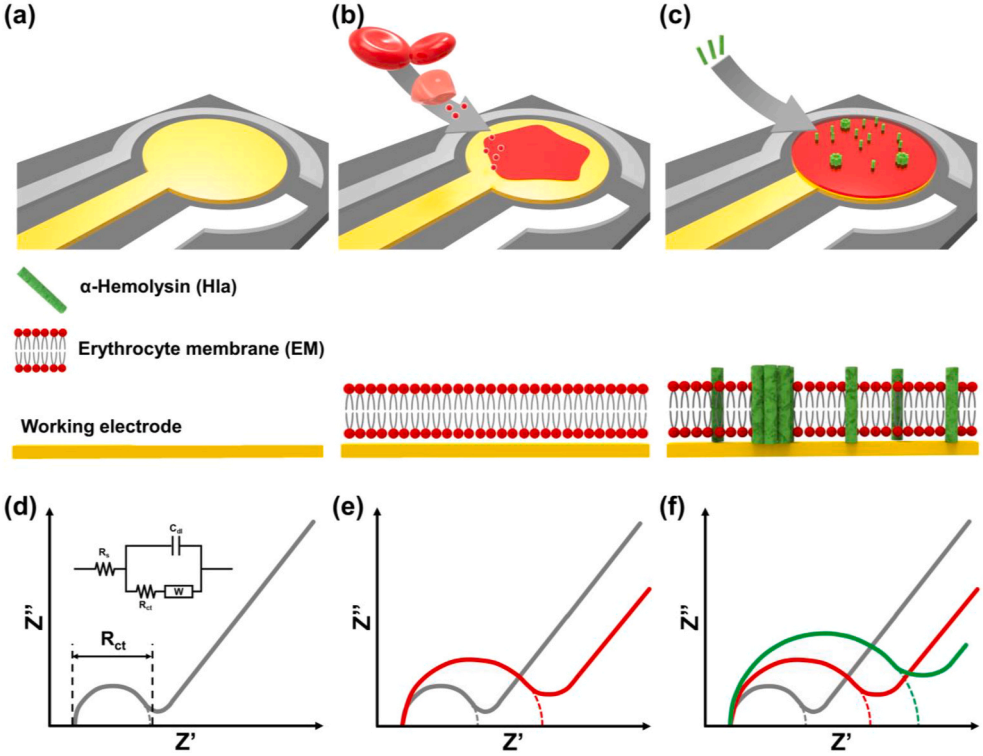

Scheme 1. (a–c) Illustration of the erythrocyte membrane-camouflaged biosensor (ECB) fabrication, detection, and corresponding side views of working electrode. (a) Bare biosensor, (b) ECB, and (c) Hla-treated ECB (Hla@ECB). Illustration for Nyquist curves of (d) bare biosensor, (e) ECB, and (f) Hla@ECB. Inset in (d) represents an equivalent circuit of the biosensor.

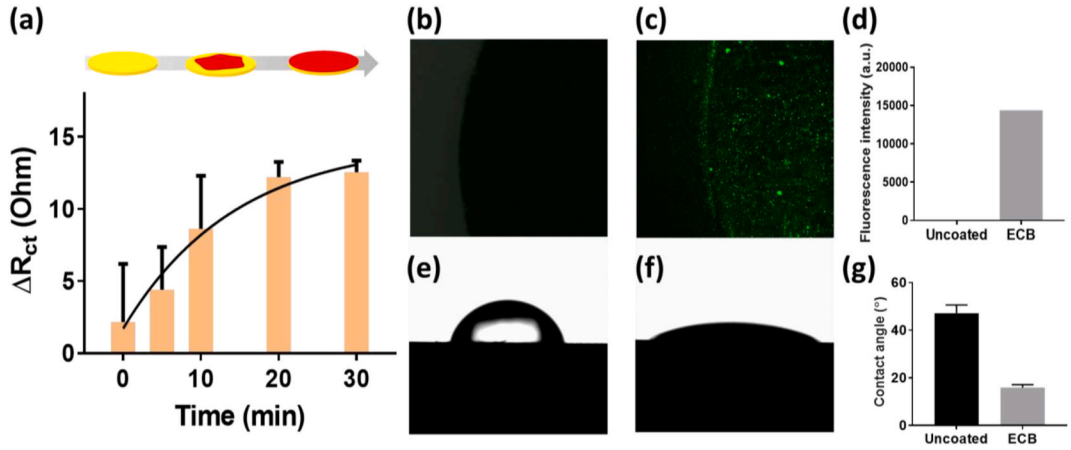

Fig. 1. Optimization and verification of EM functionalization on the surface of working electrode. (a) The ΔR_{ct} in respect of incubation time. (b–d) Fluorescence images of the uncoated sensor and the ECB. (e–g) Contact angle analysis of the uncoated sensor and the ECB.

EM-coated electrode was analyzed (Fig. 1e–g). The contact angle of bare and EM-coated working electrode was 47.1 ± 3.5° and 15.9 ± 1.3°, respectively. When EM was coated onto the working electrode, the contact angle reduced by 33.7%, which indicates that the hydrophilic phospholipid head of EM decreased the surface tension of the electrode.

3.3. Topographic analysis of the EM via AFM

To demonstrate the binding of Hla onto the EM, the surface topologies of EM and Hla-bound EM (Hla@EM) coated on mica were observed by AFM using non-contact mode imaging (Fig. 2). Hla@EM was prepared by incubation with 0.1 mg/ml Hla for 30 min at 37 °C and washing with distilled water to remove residual Hla. The AFM images and height profile showed that the EM was highly smooth and even, which implicates the single layer of EM was uniformly coated. Similarly, the AFM image showed that the EM was stably coated for 35 days (Fig. S5). For a topographical analysis, the EM was stored at 4 °C for 35 days.

In contrast, the topology of Hla@EM was rough, and had bumps, which were speculated as being Hla. The heights of the bumps were verified from the height profiles of each AFM image. The bumps were about 1 nm in height (Fig. 2b and d). It is also confirmed that the peak of the height distribution of Hla@EM was increased by 0.6 nm, compared with that of the EM (Fig. S3). The root-mean-squared roughness (R_q) of EM was 0.07 ± 0.02 nm; on the other hand, that of Hla@EM was 0.17 ± 0.03 nm, showing an increase of 2.4 times after the binding of 0.1 mg/ml Hla (Fig. S4). The topographical analysis *via* AFM verified that the Hla spontaneous bound EM with 30 min of incubation, and the Hla bound on EM, were both about 1 nm in height.

3.4. Electrochemical characterization of the ECB

To characterize the electrochemical properties, EIS for control (bare sensor), ECB, and Hla@ECB were analyzed. Fig. 3a shows the Nyquist

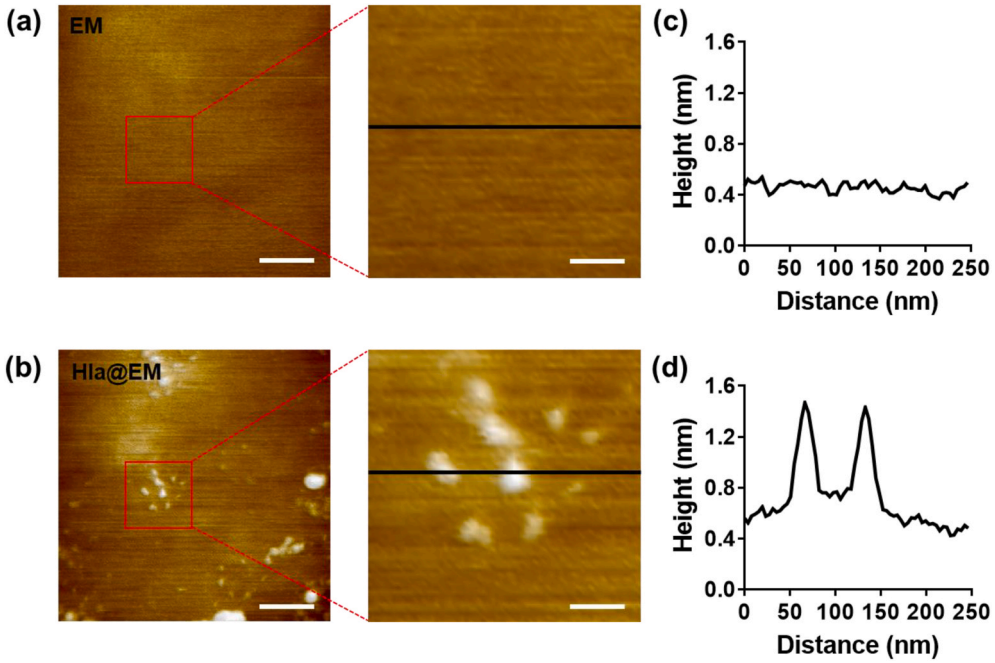

Fig. 2. AFM images of (a) a single layer of EM and (b) Hla@EM coated on mica (scale bar = 200 nm). Magnified AFM images of EM and Hla@EM, each red box in (a) and (b), respectively (scale bar = 50 nm). Height profile of (c) EM and (d) Hla@EM, according to the black solid line in the magnified AFM images, respectively. (For interpretation of the references to colour in this figure legend, the reader is referred to the Web version of this article.)

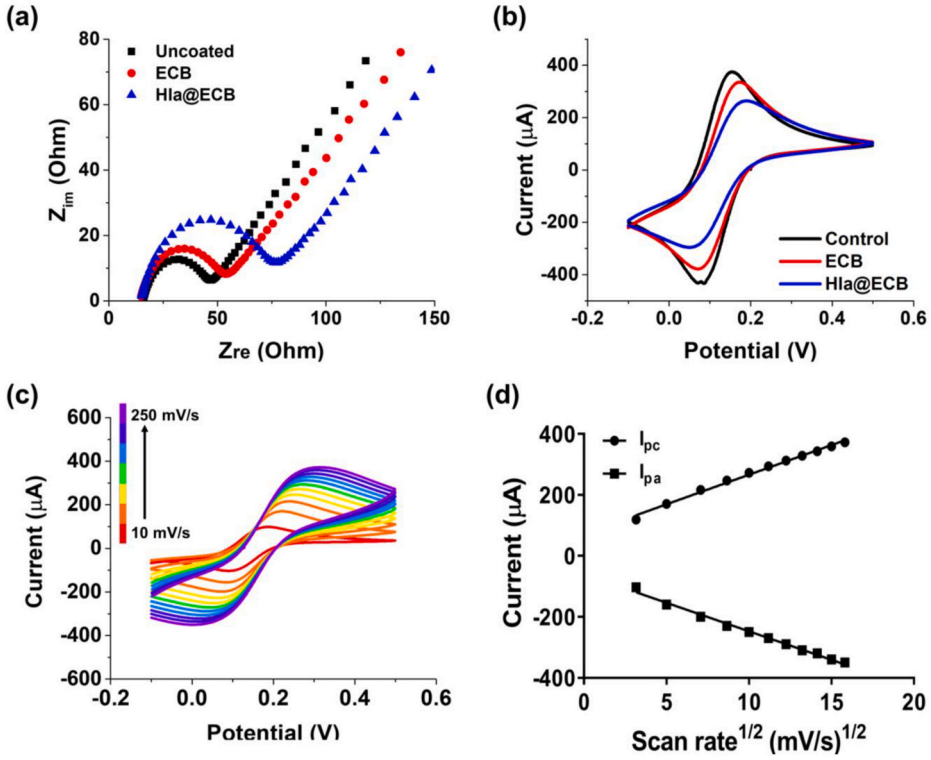

Fig. 3. Characterization of the electrochemical properties of ECB. (a) Nyquist curves of the control (bare biosensor), the ECB, and the Hla@ECB with 1 × PBS (pH 7.4) containing 0.1 M KCl, 0.5 mM $[Fe(CN)_6]^{3-}$, and 0.5 mM $[Fe(CN)_6]^{4-}$; Bare biosensor (Black square), ECB (Red circle), Hla@ECB (Blue triangle). (b) Cyclic voltammetry of each biosensor. (c) CV curves of the ECB with different scan rates ranging 10–250 mV/s. (d) Plot of cathodic (I_{pc}) and anodic peak currents (I_{pa}) vs. square root of the scan rate measured in (c). (For interpretation of the references to colour in this figure legend, the reader is referred to the Web version of this article.)

plots of each sensor (Faria and Zucolotto 2019). It is shown that the R_{ct} increases as EM and Hla are serially bound to the biosensors; the R_{ct} values for the control, ECB, and Hla@ECB (0.1 mg/ml) were 24.2 ± 1.1, 36.8 ± 0.8, and 60.4 ± 2.4 Ohm, respectively. The CV curves of each sensor were measured at the scan rate of 100 mV/s (Fig. 3b). The peak currents of the voltammogram of ECB and Hla@ECB were verified to be slightly reduced from that of control, because the electron transfer was reduced, *via* the binding of EM and Hla. The peak currents of control, ECB, and Hla@ECB were 375.2, 335.7, and 264.2 μA. CV curves of different scan rates of 10–250 mV/s were examined, and its cathodic and anodic peak currents were plotted (Fig. 3c and d). It is confirmed that the peak currents increase in proportion to the (scan rate)$^{1/2}$, which follows the Randles–Sevcik equation (Verma et al., 2020).

3.5. Sensitive and selective detection of Hla using the ECB

To verify the sensing performance of ECB, EIS was tried with Hla-spiked PBS (Fig. 4). R_{ct} increased in 21.6, 61.8, 99.4, 133.5, and 171.4 Ohm for 0.0001–1 mg/ml Hla, respectively. The results demonstrated that R_{ct} of ECB and the concentration Hla of 0.0001–1 mg/ml have an exponential relationship. Therefore, the semi-log regression for R_{ct} vs. Hla was analyzed; the R_{ct} (Ohm) = 37.1 × log(x) + 215.1 with high correlation (R^2 = 0.9993). The detection limit of ECB, calculated from 3 times the signal-to-noise ratio (3σ), was 1.9 ng/ml. The dynamic range of ECB was from 0.0001 to 1 mg/ml. Unlike our previous study of seizing target molecules with membrane receptor (Jo et al., 2019), Hla spontaneously penetrated into EM with high affinity and wide binding site, enabling highly sensitive detection. The selectivity of ECB was validated by measuring major blood proteins, such as Fib, GG, and HSA with the same concentration (Fig. 4c). Similar results were achieved by measuring 0.01 mg/ml of protein. The normalized intensities of Fib, GG, and HSA were 8.8 ± 2.8, 10.5 ± 5.9, and 12.7 ± 4.5%, respectively. As a result, it is implied that the selectivity of ECB was high enough to distinguish the toxic molecule from blood proteins.

3.6. Hla detection in human serum and its long-term stability

To detect Hla in human serum, Hla was spiked into human serum at 0.0001–1 mg/ml. Unlike PBS, human serum contains tremendous molecules, such as organic metabolites, lipids, and various proteins. Some of the molecules may interfere with the electrochemical detection of Hla through non-specific binding to EM. Intriguingly, Hla solubilized in human serum was detected with ECB, and the tendency was similar to that of Hla solubilized in PBS (Fig. 5a). It is found that the R_{ct} of ECB was exponentially increased as Hla concentration increases in the range of 0.0001–1 mg/ml. In the semi-log regression, the relation between R_{ct}

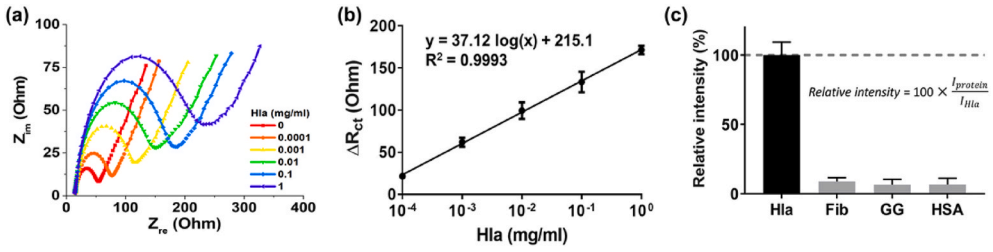

Fig. 4. The sensitive detection of Hla using ECB. (a) Nyquist curves for Hla detection of 0.0001–1 mg/ml (b) ΔR_{ct}, according to the concentration of Hla. Each data point represents quintuplicate measurements. ΔR_{ct} and Hla show a semi-log linear relationship. (c) The selectivity of ECB against major blood proteins. Relative intensity of the ECB for 0.01 mg/ml of each protein. The $I_{protein}$ and I_{Hla} represent the signal intensity of ECB for protein and Hla sample, respectively. Abbreviation note: Fib = fibrinogen; GG = gamma globulin; HSA = human serum albumin.

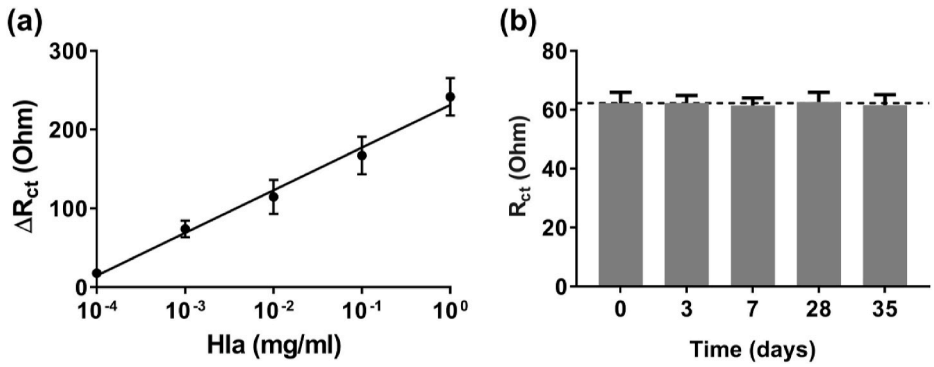

Fig. 5. (a) Detection of the Hla spiked in human serum at 0.0001–1 mg/ml. (b) R_{ct} of the ECBs stored for 0–35 days measuring 0.01 mg/ml Hla.

and the concentration of Hla was found to be R_{ct} (Ohm) = 54.1 × log(x) + 231.2 (R^2 = 0.9894). It is speculated that a few amounts of serum proteins, such as GG and HSA, bind onto ECB. As a result, the linearity was reduced by about 1%. Finally, the stability of ECB was tested (Fig. 5b). The ECBs were stored at 4 °C for 35 days and used to measure 0.01 mg/ml Hla. The R_{ct} of ECB was highly consistent, regardless of the days of storage. As a result, the relative signal for 0.01 mg/ml Hla was 100.1 ± 5.9, 100.1 ± 4.0, 98.7 ± 4.1, 100.6 ± 5.2, and 99.0 ± 5.6% for 3, 7, 28, and 35 days, respectively. These results are well consistent with the long-term stability test of ECB by fluoroscopic analysis of the EM on the electrode for 35 days (Fig. S6).

3.7. Clinical sample test using the ECB

The average ΔR_{ct} values of blood samples from 5 patients with *S. aureus* bacteremia and from 4 patients without *S. aureus* bacteremia were 116.92 ± 24.41 and 44.38 ± 11.14 Ohm, respectively (Fig. S7). The ΔR_{ct} values between the two groups showed statistically significant (p = 0.00114), demonstrating that the ECB can distinguish the *S. aureus* bacteremia from healthy conditions.

4. Conclusion

In summary, we took advantage of EM for the selective detection of Hla secreted from *S. aureus* and MRSA. Electrochemical sensors were coated with EM for camouflaging erythrocyte. The bacterial toxins were verified by AFM to spontaneously bind to the EM, as well as erythrocyte. The electrochemical signal was proportional (R^2 = 0.9993) to the concentration of Hla in the detection range of 0.0001–1 mg/ml with semi-logarithmic scale. ECBs showed high sensitivity of 1.9 ng/ml, and had selectivity to Hla against fib, GG, and HSA. In this regard, the signal for Hla was 14.1, 9.8, and 15.4 times higher than that of the same concentration of Fib, GG, and HSA, respectively. Remarkably, human serum containing various interfering substances demonstrated similar sensing performance of ECB. The ECBs were also verified to be highly stable for 5 weeks storage, exhibiting 1% errors from freshly made ECBs for measuring Hla, because EM had barely degraded over a long period of time. Noted that although the ECB successfully detected Hla against major blood proteins, further thorough investigation about selectivity with various molecules in blood should be required prior to commercialization. Nevertheless, our sensing strategy and findings shed light on the ECB for Hla detection technique as a rapid and accurate point-of-care test for bacterial infection. Furthermore, the sensing mechanism of this study could be applied to detect other pathogens using other origin of cell membrane.

CRediT authorship contribution statement

Insu Kim: Investigation, Conceptualization, Methodology, Visualization, Writing, Formal analysis, Writing – original draft, Writing – review & editingediting, Cell membrane extraction. **Yonghwan Kim:** Investigation, Methodology, Visualization, Writing – editing. **Sang Won Lee:** Atomic force microscopy and Writing. **Dongtak Lee:** Atomic force microscopy. **Hyo Gi Jung:** Atomic force microscopy. **Jae Won Jang:** Cell culture and Cell membrane extraction. **Taeha Lee:** Technique support. **Young Kyung Yoon:** Clinical sample test, Interpretation of clinical data. **Gyudo Lee:** Writing – review & editing. **Dae Sung Yoon:** Supervision, Writing – review & editing.

Declaration of competing interest

The authors declare that they have no known competing financial interests or personal relationships that could have appeared to influence the work reported in this paper.

Acknowledgement

This work was supported by the National Research Foundation of Korea (NRF) Grant funded by the Korean Government (MSIP) (No., NRF-2018M3C1B7020722, NRF-2019R1A2B5B01070617, and NRF-2020R1A6A3A01096477). This work was supported by the Korea Medical Device Development Fund grant funded by the Korea government (the Ministry of Science and ICT, the Ministry of Trade, Industry and Energy, the Ministry of Health & Welfare, the Ministry of Food and Drug Safety) (Project Number: 202012D19). This study was also supported by the BK21 FOUR (Fostering Outstanding Universities for Research).

Appendix A. Supplementary data

Supplementary data to this article can be found online at https://doi.org/10.1016/j.bios.2021.113267.

References

Castellana, E.T., Cremer, P.S., 2006. Surf. Sci. Rep. 61 (10), 429–444.
Cattoir, V., Merabet, L., Djibo, N., Rioux, C., Legrand, P., Girou, E., Lesprit, P., 2011. Clin. Microbiol. Infect. 17 (3), 425–431.
Divyakolu, S., Chikkala, R., Ratnakar, K.S., Sritharan, V., 2019. Adv. Infect. Dis. 9 (2), 80–104.
Escajadillo, T., Olson, J., Luk, B.T., Zhang, L., Nizet, V., 2017. Front. Pharmacol. 8 (477).
Esteban-Fernández de Ávila, B., Angsantikul, P., Ramírez-Herrera, D.E., Soto, F., Teymourian, H., Dehaini, D., Chen, Y., Zhang, L., Wang, J., 2018. Sci. Robot. 3 (18), eaat0485.
Evans, B.C., Nelson, C.E., Yu, S.S., Beavers, K.R., Kim, A.J., Li, H., Nelson, H.M., Giorgio, T.D., Duvall, C.L., 2013. JoVE (73) e50166-e50166.
Faria, H.A.M., Zucolotto, V., 2019. Biosens. Bioelectron. 131, 149–155.
Ferhan, A.R., Yoon, B.K., Park, S., Sut, T.N., Chin, H., Park, J.H., Jackman, J.A., Cho, N. J., 2019. Nat. Protoc. 14 (7), 2091–2118.
Fischer, L.M., Tenje, M., Heiskanen, A.R., Masuda, N., Castillo, J., Bentien, A., Émneus, J., Jakobsen, M.H., Boisen, A., 2009. Microelectron. Eng. 86 (4), 1282–1285.
Foster, T.J., 2017. FEMS Microbiol. Rev. 41 (3), 430–449.

Gao, W., Hu, C.-M.J., Fang, R.H., Luk, B.T., Su, J., Zhang, L., 2013. Adv. Mater. 25 (26), 3549–3553.
González-Sánchez, M.I., Gómez-Monedero, B., Agrisuelas, J., Iniesta, J., Valero, E., 2019. J. Electroanal. Chem. 839, 75–82.
Hu, C.-M.J., Fang, R.H., Copp, J., Luk, B.T., Zhang, L., 2013. Nat. Nanotechnol. 8 (5), 336–340.
Jo, S., Kim, I., Lee, W., Kim, M., Park, J., Lee, G., Yoon, D.S., Park, J., 2019. Biosens. Bioelectron. 135, 216–223.
Kim, I., Kim, C., Lee, D., Lee, S.W., Lee, G., Yoon, D.S., 2020. Analyst 145 (6), 2125–2132.
Kim, I., Kwon, D., Lee, D., Lee, G., Yoon, D.S., 2019. Biosens. Bioelectron. 135, 82–87.
Kim, I., Kwon, D., Lee, D., Lee, T.H., Lee, J.H., Lee, G., Yoon, D.S., 2018. Biosens. Bioelectron. 102, 617–623.
Kim, I., Lee, D., Lee, S.W., Lee, J.H., Lee, G., Yoon, D.S., 2021. ACS Nano in Press 15 (4), 6386–6394.
Kumar, S., Han, J.-A., Michael, I.J., Ki, D., Sunkara, V., Park, J., Gautam, S., Ha, H.K., Zhang, L., Cho, Y.-K., 2019. Adv. Funct. Mater. 29 (30), 1970205.
Mingeot-Leclercq, M.-P., Deleu, M., Brasseur, R., Dufrêne, Y.F., 2008. Nat. Protoc. 3 (10), 1654–1659.
Park, J., Lee, W., Kim, I., Kim, M., Jo, S., Kim, W., Park, H., Lee, G., Choi, W., Yoon, D.S., Park, J., 2019. Sensor. Actuator. B Chem. 293, 296–303.
Russell, C., Ward, A.C., Vezza, V., Hoskisson, P., Alcorn, D., Steenson, D.P., Corrigan, D. K., 2019. Biosens. Bioelectron. 126, 806–814.
Sekiguchi, K., Saito, M., Yajima, R., 1995. Microbiol. Immunol. 39 (8), 545–550.
Soule, D.W., Marinetti, G.V., Morgan, H.R., 1959. J. Exp. Med. 110 (1), 93–102.
Sun, L., Chen, Y., Wang, D., Wang, H., Wu, D., Shi, K., Yan, P., Yu, Y., 2019. Emerg. Infect. Dis. 25 (1), 157–160.
Tabaei, S.R., Choi, J.-H., Haw Zan, G., Zhdanov, V.P., Cho, N.-J., 2014. Langmuir 30 (34), 10363–10373.
Tanaka, M., Sackmann, E., 2005. Nature 437 (7059), 656–663.
Tong, S.Y.C., Davis, J.S., Eichenberger, E., Holland, T.L., Fowler, V.G., 2015. Clin. Microbiol. Rev. 28 (3), 603–661.
Turner, N.A., Sharma-Kuinkel, B.K., Maskarinec, S.A., Eichenberger, E.M., Shah, P.P., Carugati, M., Holland, T.L., Fowler, V.G., 2019. Nat. Rev. Microbiol. 17 (4), 203–218.
Verma, S., Arya, P., Singh, A., Kaswan, J., Shukla, A., Kushwaha, H.R., Gupta, S., Singh, S.P., 2020. Biosens. Bioelectron., p. 112347
Yadav, S.P., Ahmad, A., Pandey, B.K., Verma, R., Ghosh, J.K., 2008. Biochemistry 47 (7), 2134–2142.